16. D. W. Lea, *J. Clim.* **17**, 2170–2179 (2004).
17. T. Sagawa, Y. Yokoyama, M. Ikehara, M. Kuwae, *Geophys. Res. Lett.* **38**, L00F02 (2011).
18. P. N. DiNezio *et al.*, *Paleoceanography* **26**, PA3217 (2011).
19. D. H. Andreasen, A. C. Ravelo, *Paleoceanography* **12**, 395–413 (1997).
20. J. Xu, W. Kuhnt, A. Holbourn, M. Regenberg, N. Andersen, *Paleoceanography* **25**, PA4230 (2010).
21. P. Fiedler, L. Talley, *Prog. Oceanogr.* **69**, 143–180 (2006).
22. K. Thirumalai, J. W. Partin, C. S. Jackson, T. M. Quinn, *Paleoceanography* **28**, 401–412 (2013).
23. E. C. Brady, B. L. Otto-Bliesner, J. E. Kay, N. Rosenbloom, *J. Clim.* **26**, 1901–1925 (2013).
24. A. Patrick, R. Thunell, *Paleoceanography* **12**, 649–657 (1997).
25. H. Spero, K. Mielke, E. Kalve, D. Lea, D. Pak, *Paleoceanography* **18**, 1022 (2003).
26. D. Rincón-Martínez, S. Steph, F. Lamy, A. Mix, R. Tiedemann, *Mar. Micropaleontol.* **79**, 24–40 (2011).
27. H. M. Benway, A. C. Mix, B. A. Haley, G. P. Klinkhammer, *Paleoceanography* **21**, PA3008 (2006).
28. A. Koutavas, J. Lynch-Stieglitz, T. M. Marchitto Jr., J. P. Sachs, *Science* **297**, 226–230 (2002).
29. G. E. Manucharyan, A. V. Fedorov, *J. Clim.* **27**, 5836–5850 (2014).
30. Z.-Z. Hu *et al.*, *J. Clim.* **26**, 2601–2613 (2013).
31. M. Collins *et al.*, *Nat. Geosci.* **3**, 391–397 (2010).
32. N. A. Rayner *et al.*, *J. Geophys. Res.* **108**, 4407 (2003).

ACKNOWLEDGMENTS

We thank P. DiNezio, A. Fedorov, B. Hönisch, G. Manucharyan, A. Moore, A. Paytan, J. Zachos, and two anonymous reviewers for comments on the manuscript. R. Franks, E. Chen, J. Hourigan, and N. Movshovitz provided analytical support. For this research, we used samples provided by the Integrated Ocean Drilling Program (IODP). Funding for this research was provided by NSF grant OCE-1204254 (A.C.R.), the Achievement Rewards for College Scientists Foundation (H.L.F.), and the Schlanger Fellowship (H.L.F), which is part of the NSF-sponsored U.S. Science Support Program for IODP that is administered by the Consortium for Ocean Leadership. Our data are deposited at the National Oceanic and Atmospheric Administration National Climatic Data Center and Pangaea.

SUPPLEMENTARY MATERIALS

www.sciencemag.org/content/347/6219/255/suppl/DC1
Materials and Methods
Supplementary Text
Figs. S1 to S17
Tables S1 to S3
References (*33*–*70*)

7 July 2014; accepted 11 December 2014
10.1126/science.1258437

PALEOECOLOGY

Linked canopy, climate, and faunal change in the Cenozoic of Patagonia

Regan E. Dunn,[1]* Caroline A. E. Strömberg,[1] Richard H. Madden,[2] Matthew J. Kohn,[3] Alfredo A. Carlini[4]

Vegetation structure is a key determinant of ecosystems and ecosystem function, but paleoecological techniques to quantify it are lacking. We present a method for reconstructing leaf area index (LAI) based on light-dependent morphology of leaf epidermal cells and phytoliths derived from them. Using this proxy, we reconstruct LAI for the Cenozoic (49 million to 11 million years ago) of middle-latitude Patagonia. Our record shows that dense forests opened up by the late Eocene; open forests and shrubland habitats then fluctuated, with a brief middle-Miocene regreening period. Furthermore, endemic herbivorous mammals show accelerated tooth crown height evolution during open, yet relatively grass-free, shrubland habitat intervals. Our Patagonian LAI record provides a high-resolution, sensitive tool with which to dissect terrestrial ecosystem response to changing Southern Ocean conditions during the Cenozoic.

Vegetation structure—the degree of canopy openness—is a fundamental aspect of ecosystems, influencing productivity, hydrological and carbon cycling, erosion, and composition of faunal communities (*1*, *2*). However, methods to quantify ancient vegetation structure have eluded paleoecologists. Here, we present a method with which to reconstruct vegetation openness, specifically leaf area index [LAI = foliage area (m^2)/ground area (m^2)], using the morphology of leaf epidermal cells preserved as phytoliths (plant biosilica) (Fig. 1). LAI quantifies vegetation structure in ecological and climate modeling studies (*1*, *3*). In modern ecosystems, LAI relates primarily to soil moisture (*4*), by which vegetation becomes more closed with increasing soil water availability; ultimately, soil moisture is determined by temperature, precipitation, and atmospheric partial pressure of CO_2 (P_{CO_2}) (*4*, *5*). Disturbance in the form of fire and herbivory can offset this relationship, resulting in open habitats in areas with relatively high rainfall (*6*).

Using this paleobotanical archive, we reconstructed a LAI record for the middle Cenozoic [49 million to 11 million years ago (Ma)] of Patagonia to test predictions about vegetation

[1]Department of Biology and Burke Museum of Natural History and Culture, University of Washington, Seattle, WA 98195, USA. [2]Department of Organismal Biology and Anatomy, University of Chicago, Chicago, IL 60637, USA. [3]Department of Geosciences, Boise State University, Boise, ID 83725, USA. [4]Paleontología de Vertebrados, Universidad Nacional de La Plata, Consejo Nacional de Investigaciones Científicas y Técnicas (CONICET), La Plata, Argentina.
*Corresponding author. E-mail: dunnr@u.washington.edu

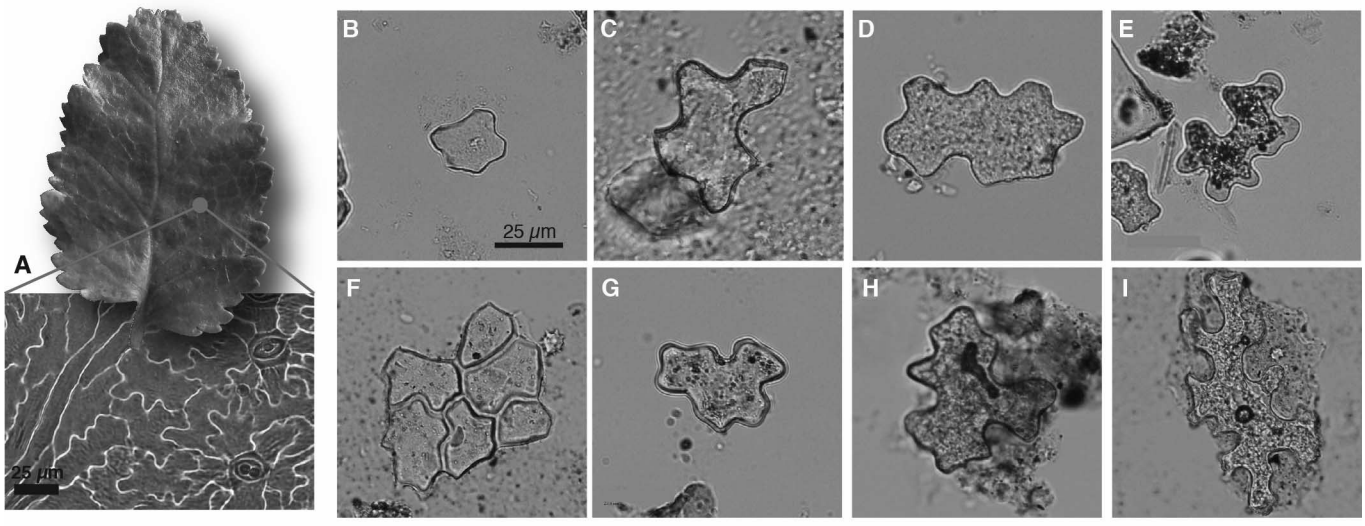

Fig. 1. Leaf epidermis and examples of epidermal phytoliths. (**A**) *Nothofagus* leaf and epidermis. (**B** to **E**) Fossil phytoliths from Patagonia. (**F** to **I**) Modern soil phytoliths from Costa Rica.

response to Cenozoic climate fluctuations and how changes in vegetation structure relate to the evolution of high-crowned (hypsodont) and ever-growing (hypselodont) tooth morphologies in South American herbivores (*7*).

Climatic cooling beginning in the middle Eocene (49 Ma) and major warming events in the late Oligocene (~26 Ma) and middle Miocene (17 to 14 Ma) (*8*) have been linked to tectonics, ocean circulation (*9*), atmospheric P_{CO_2} (*10*), and ice volume after the onset of extensive Antarctic glaciation at the Eocene–Oligocene Transition (EOT; 33.9 Ma) (*8*). A narrow landmass, Patagonia is sensitive to Southern Ocean climate and provides an ideal test case for the influence of global climate on vegetation structure.

It has long been assumed that hypsodonty in endemic South American herbivores beginning in the middle Eocene (~40 Ma) evolved in response to the spread of Earth's first grasslands (*11*), but recent work found that grasses were rare (*12*). When grasses are rare, "traditional" phytolith analysis cannot resolve habitat openness (*13*, *14*), so it has remained unclear whether hypsodonty evolved in forests or in open but grass-free habitats, possibly in conjunction with tooth abrasion during ingestion of exogenous grit (*12*).

Our proxy for reconstructing ancient LAI [reconstructed LAI (rLAI)] is based on the well-known influence of sunlight on the size and shape of pavement cells in leaf epidermis (Fig. 1A). In shade, these cells are larger and have more undulated outlines than those of cells exposed to full sun (*15*, *16*). Silica mineralization produces a precision cast of pavement cells in living plants that can be preserved as fossils (Fig. 1B). Because sunlight filtering through a canopy is a function of LAI, we hypothesized that leaf epidermal cells and their phytoliths are on average larger and more undulated in closed forests than in open habitats and that the relationship is linear across a canopy density gradient. Because these phytolith types are taxonomically nondiagnostic we cannot control for phylogenetic variation in cell morphology. Instead, we tested our hypotheses using modern assemblages of phytoliths extracted from soils collected across an LAI gradient from 0 (completely open) to 5 (dense forest) in Costa Rica (Fig. 1C).

Cenozoic-aged floras from Patagonia contain a nonanalog mix of mesic and xeric taxa of tropical and sub-Antarctic lineages (such as Arecaceae, Anacardiaceae, Fabaceae, Zingiberaceae, Proteaceae, *Nothofagus*, Podocarpaceae, and Araucariaceae). We chose to sample phytoliths from modern tropical soils in Costa Rica because it has wet and dry forests, savanna, and shrubby areas containing many of the reported fossil genera (41%) and families (85%) (table S1). We assume that relative change in epidermal cell morphology is based on canopy density and is independent of taxonomy and latitudinal variation in light regime. Using light microscopy, nongrass epidermal phytoliths in extracted samples were photographed and measured for the calibration data set. Phytolith undulation was standardized by using an undulation index (UI = circumference of cell/circumference of a circle with cell area) (*16*), and mean site values for phytolith UI (PUI) and phytolith area (PA) were compared with field measurements of LAI from hemispherical photographs (Fig. 2A). Measurements of fossil phytoliths followed the same protocol.

In the modern training data set of 45 sites (table S2), LAI correlates with PUI [coefficient of determination (R^2) = 0.59, $P < 0.0001$] (Fig. 2B) and PA (R^2 = 0.44, $P < 0.0001$) (Fig. 2C). A linear multiple regression analysis including both variables improves the correlation (Fig. 2D and table S3):

$$\text{rLAI} = 0.0012 \times \text{PA}(\mu\text{m}^2) + 10.4118 \times \text{PUI} - 13.1621 \quad (1)$$

(R^2 = 0.63, $P < 0.0001$, SE = 0.695, $F_{2,42}$ = 39). Using Eq. 1, we reconstructed rLAI for 46 fossil phytolith assemblages from Patagonian paleosols spanning 49 to 11 Ma (Fig. 3A, fig. S3, and

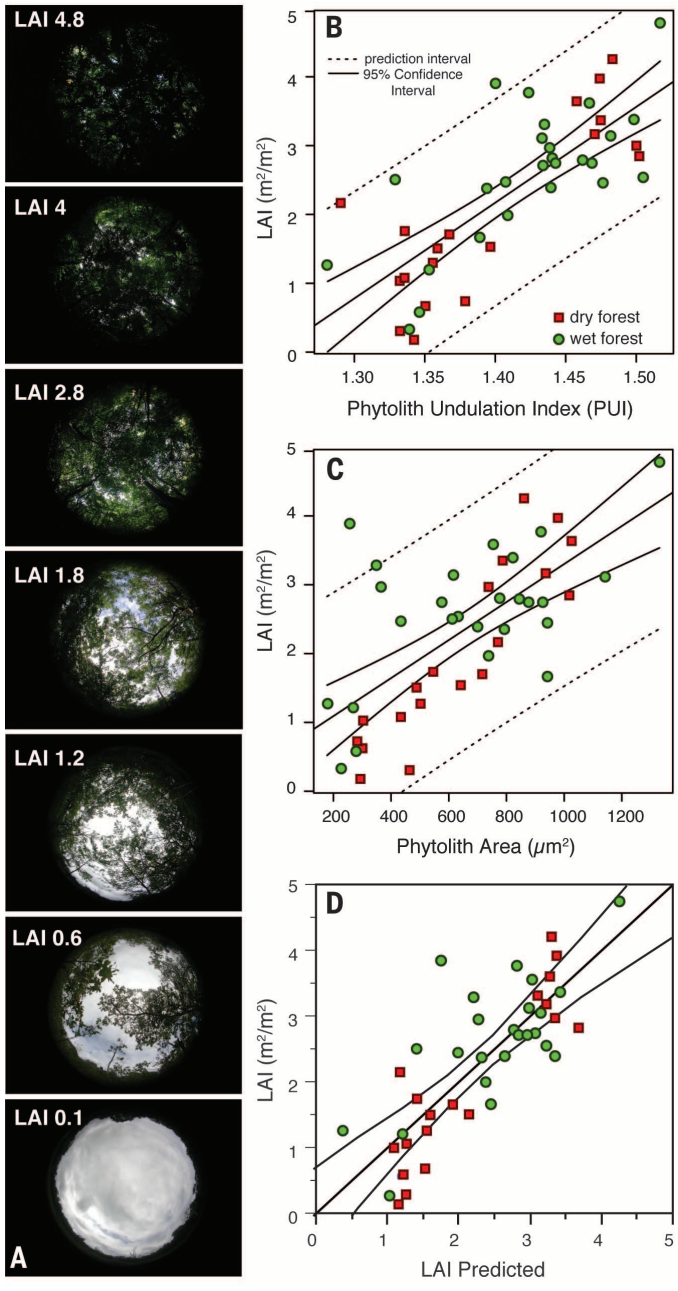

Fig. 2. Modern soil phytolith morphology and LAI. (**A**) Hemispherical photographs from Costa Rica illustrating LAI values. (**B**) Linear regressions for mean PUI and LAI (rLAI = 13.92 × PUI – 17.31); and (**C**) mean Phytolith Area (PA) and LAI (rLAI = 0.0028 × PA + 0.531). (**D**) Plot of simulated versus measured values of LAI. Simulated values are derived from Eq. 1.

table S4). Data from different times should be comparable because all samples are from the same region with the same moisture resources (for example, similar vegetation occupy all sites today). From the middle Eocene to early Oligocene (49.0 to 32.3 Ma), rLAI values decline from ~4 to 0.6, indicating an opening of the landscape, from dense vegetation (such as broadleaf forest; LAI = 4 to 3) to progressively more open vegetation (such as dry forest, woodland, and scrub; LAI = 2 to 1); and last, to very open habitats (such as shrubland or desert; LAI < 1) (Table 1 and Fig. 3). High rLAI values during the middle Eocene correspond in age with the highly diverse megathermal floras 380 km farther north (*17*), and middle Eocene–early Oligocene decreases in rLAI correspond with increased abundances of sub-Antarctic taxa such as *Nothofagus* (*18*, *19*).

Between 38.5 and 38.0 Ma and 35.0 and 32.2 Ma, habitats were maximally open (rLAI <1). Diagnostic phytoliths from these assemblages indicate abundant palms, woody eudicotyledons, and sparse grasses (<1 to 15%) (*12*). We interpret these habitats as a nonanalog palm shrubland with a discontinuous canopy. During the late Oligocene, rLAI increases, indicating dry forest, woodland, or scrub until the earliest Miocene (~21.1 and 18.8 Ma), when rLAI drops again. Early Miocene rLAI fluctuations (<1 to 2.4) suggest shifts between palm shrubland and open forest without a continuous grassy understory (*12*). The middle Miocene (~15.7 to 14.6 Ma) saw a brief spike in rLAI values (>3.5) at 14.6 Ma, after which (~14.2 Ma) rLAI values trend downward again. Pollen records from late Oligocene–middle Miocene marine strata of Patagonia indicate humid forest conditions dominated by *Nothofagus* and podocarps, with low abundances of arid-adapted (inferred as open habitat) taxa before 10 Ma (*20*). These pollen data do not contradict our findings because they reflect regional vegetation and are biased toward prolific pollen producers, whereas our phytolith samples represent in situ vegetation of the central Patagonian lowlands.

Broad changes in rLAI track the Southern Ocean $\delta^{18}O$ temperature record (*8*, *21*); rLAI decreases during mid–late Eocene cooling and increases during late Oligocene warming. The middle Miocene (~15.7 to 14.6 Ma) regreening of Patagonia coincides with increased atmospheric Pco_2 (*22*) and reduced Antarctic ice sheet volume (*23*). After ~14.2 Ma, declining rLAI values are consistent with middle Miocene cooling, ice-growth, and modeled changes in meridional heat and vapor transport (*24*).

Vegetation-climate decoupling occurred during pulses of maximum openness at 38.5 to 38.0 Ma and at ~35 Ma, as marine temperatures gradually declined. This second pulse predates the EOT by >1 million years; in contrast, during abrupt EOT cooling, rLAI remained relatively unchanged. Quasi-constant rLAI during the EOT is consistent with phytolith abundance data, suggesting compositionally stable vegetation (*12*) and isotopically inferred invariant temperatures (*25*). However, aeolian sedimentation rates dramatically increased at 33.6 Ma (*26*), which is consistent with Oi-1 glaciation.

Intervals of open vegetation likely reflect reduced precipitation, although disturbance such as fire, volcanism, or herbivory may have contributed. Megafloral records from elsewhere in

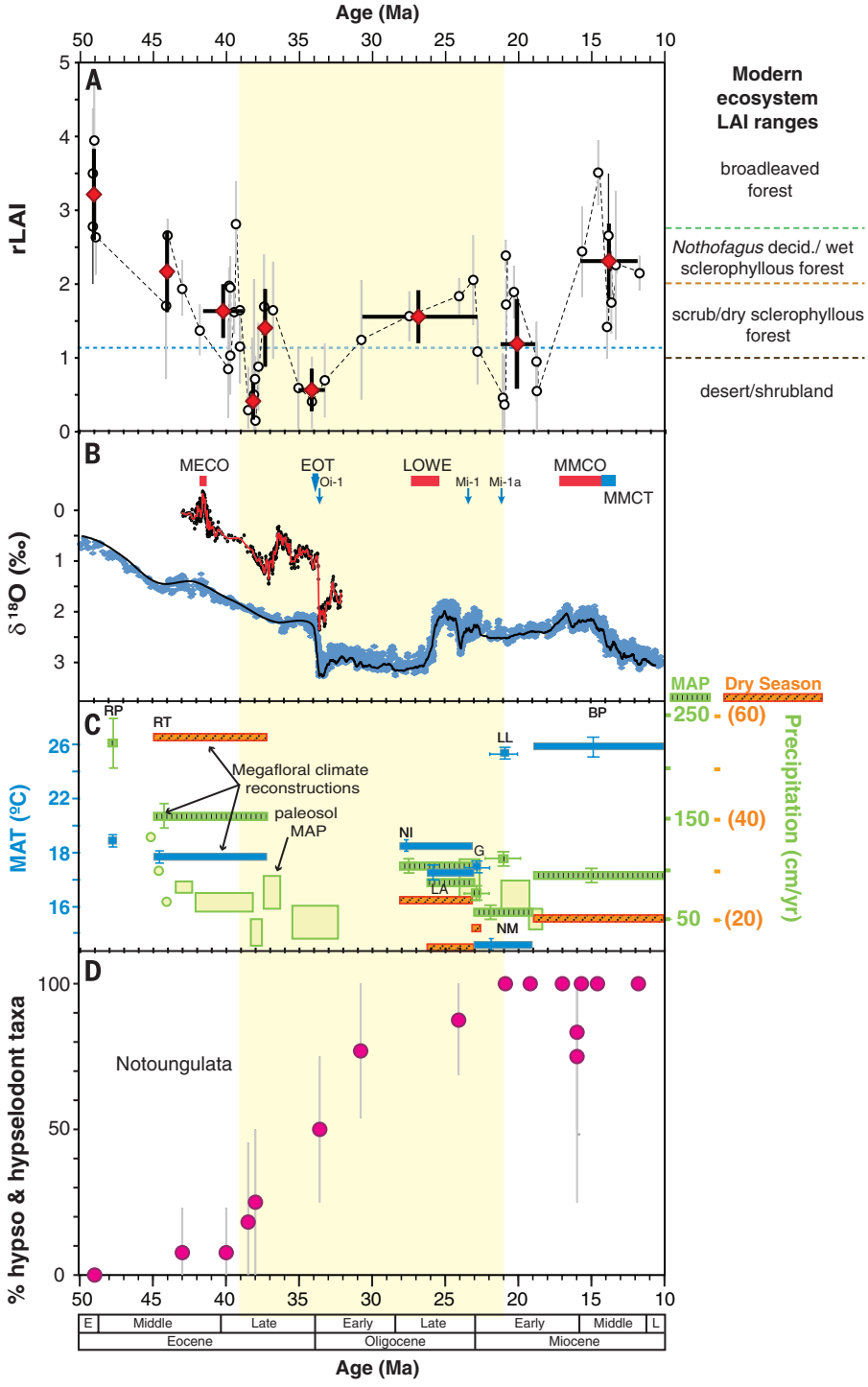

Fig. 3. Middle Cenozoic rLAI and comparisons to climate and biotic records. (**A**) rLAI reconstruction with 95% confidence intervals. Shown are raw values (open circles) and binned values by age or geologic unit (red diamonds) (table S4). (**B**) Foraminiferal $\delta^{18}O$ records for sea surface (red) (*21*) and deep sea temperature (blue) (*8*). (**C**) MAT (blue), MAP (green), and dry-season precipitation (orange) estimates from megafloras (*27*, *33*), with corrected ages (table S5). Length of the solid bars indicate age uncertainty. Yellow boxes are MAP estimates from paleosols (*34*). (**D**) Proportion hypsodont+hypselodont taxa of notoungulates, with 95% confidence intervals (table S6).

Table 1. Modern habitat LAI ranges from literature. Dashes indicate no reported data.

Biome type	Mean LAI	Minimum	Maximum	Reference
Wetlands	6.30	2.5	8.4	(*1*)
Tropical evergreen broad	4.80	1.5	8	(*1*)
Temperate evergreen broadleaf	4.33	0.8	11.6	(*1*, *35*)
Tropical deciduous broadleaf	3.90	0.6	8.9	(*1*)
Temperate deciduous broadleaf	3.56	0.6	5.08	(*1*, *35*)
Nothofagus evergreen	3.50	2.5	4.5	(*36*)
Nothofagus deciduous	2.55	2.3	2.8	(*36*)
Sclerophyllous forest Australia	2.40	—	—	(*37*)
Grasslands	1.75	0.08	5	(*1*, *35*)
Monte	1.70	0.5	2.9	(*38*)
Mediterranean scrub	1.50	1	4	(*39*)
Chaco (dry forest)	1.5	1	3	(*40*)
Savanna	1.49	0.78	1.72	(*35*)
Sclerophyllous forest Australia	0.95	—	—	(*37*)
Shrublands	0.77	0.1	4.5	(*1*, *35*, *38*)
Desert	0.55	0.9	0.2	(*1*)

Patagonia document stable mean annual temperatures (MATs) of ~18°C, but decreasing mean annual precipitation (MAP) from the middle Eocene onward (Fig. 3C) (*27*). By at least the late Oligocene, decreased MAP values reflect reduced dry-season rainfall (*27*). Locally, episodes of low rLAI correspond to the lowest MAP estimates from paleosols and shifts to aeolian sedimentation (*28*). Additionally, phytoliths of water-demanding gingers become very rare (0.4%) by 38.1 Ma and disappear after ~38 Ma (*12*). Our climate interpretation is seemingly at odds with phytolith evidence for abundant palms, which in modern South America is linked to warm, humid climates (*29*). However, Patagonian fossils indicate that a largely dry-adapted palm clade (Attaleinae) had diversified in South America by the Paleocene (fig. S5). We hypothesize that water-use efficiency in these palms was further enhanced under elevated Eocene atmospheric P_{CO_2} (*30*).

Increasing openness (rLAI < 1) ~40 Ma coincided with initiation of tooth crown height increases in several clades of notoungulates (Fig. 3D). Proportions of hypsodont+hypselodont taxa continued to rise from 38 to 20 Ma, as rLAI remained low (between 0 and 2; average ≤ 1.5). The hypsodonty trend may have reversed during more forested middle Miocene conditions, but errors are large, and constant hypsodonty proportions cannot be ruled out. In modern South American environments, the proportion of hypsodont+hypselodont species dramatically increases under a LAI value of ~1.2 (fig. S6 and table S7). These areas experience low precipitation, frequent dust storms, and erosion of tephric materials (*31*).

Evidently, feeding in drier, more open Eocene–early Miocene ecosystems provided evolutionary pressure to drive hypsodonty and hypselodonty in Patagonia. The temporal coincidence of windblown ash, low rLAI, and increased rates of hypsodonty+hypselodonty further suggests that ash played a key role in this process (*12*). In low LAI habitats today (such as shrublands), sparse vegetation includes both bare ground (dust source areas) and shrubs (traps for dust) (*32*). Thus, ingestion of dust adhering to plants growing on highly erodible surfaces (tephra-rich soils) plausibly drove this pattern of tooth evolution in South America.

Taken together, these patterns indicate that long-term climate changes that predated the EOT drove ecosystem changes in Patagonia. Specifically, we propose that Southern Ocean instability during the protracted opening of Drake Passage beginning in the middle Eocene (*9*) and associated cooling sea surface temperatures resulted in reduced rainfall on land and triggered successive opening-up of landscapes during the middle-late Eocene. Our method for estimating rLAI allows for quantification of vegetation structure through time, and because it relies on microfossils, extremely high-resolution records of habitat change are possible. Additionally, because leaf epidermis is a highly conserved tissue, the method should be applicable across a broad range of temporal scales to test many outstanding hypotheses in paleoecology.

REFERENCES AND NOTES

1. G. P. Asner, J. M. O. Scurlock, J. A. Hicke, *Glob. Ecol. Biogeogr.* **12**, 191–205 (2003).
2. R. F. Kay, R. H. Madden, C. Van Schaik, D. Higdon, *Proc. Natl. Acad. Sci. U.S.A.* **94**, 13023–13027 (1997).
3. R. Betts, P. Cox, S. Lee, F. Woodward, *Nature* **387**, 796–799 (1997).
4. O. Dermody, J. F. Weltzin, E. C. Engel, P. Allen, R. J. Norby, *Plant Soil* **301**, 255–266 (2007).
5. A. Iio, K. Hikosaka, N. P. R. Anten, Y. Nakagawa, A. Ito, *Glob. Ecol. Biogeogr.* **23**, 274–285 (2013).
6. A. C. Staver, S. Archibald, S. A. Levin, *Science* **334**, 230–232 (2011).
7. Materials and methods are available as supplementary materials on *Science* Online.
8. J. Zachos, M. Pagani, L. Sloan, E. Thomas, K. Billups, *Science* **292**, 686–693 (2001).
9. R. Livermore, C.-D. Hillenbrand, M. Meredith, G. Eagles, *Geochem. Geophys. Geosyst.* **8**, Q01005 (2007).
10. M. Pagani, J. C. Zachos, K. H. Freeman, B. Tipple, S. Bohaty, *Science* **309**, 600–603 (2005).
11. B. F. Jacobs, J. D. Kingston, L. L. Jacobs, *Ann. Mo. Bot. Gard.* **86**, 590–643 (1999).
12. C. A. E. Strömberg, R. E. Dunn, R. H. Madden, M. J. Kohn, A. A. Carlini, *Nat. Commun.* **4**, 1478 (2013).
13. C. A. E. Strömberg, *Palaeogeogr. Palaeoclimatol. Palaeoecol.* **207**, 239–275 (2004).
14. L. Bremond, A. Alexandre, C. Hély, J. Guiot, *Global Planet. Change* **45**, 277–293 (2005).
15. R. W. Watson, *New Phytol.* **41**, 223–229 (1942).
16. W. M. Kürschner, *Rev. Palaeobot. Palynol.* **96**, 1–30 (1997).
17. P. Wilf *et al.*, *Am. Nat.* **165**, 634–650 (2005).
18. V. Barreda, L. Palazzesi, *Bot. Rev.* **73**, 31–50 (2007).
19. E. J. Romero, *Ann. Mo. Bot. Gard.* **73**, 449–461 (1986).
20. L. Palazzesi, V. Barreda, *Nat. Commun.* **3**, 1294 (2012).
21. S. M. Bohaty, J. C. Zachos, *Geology* **31**, 1017–1020 (2003).
22. Y. G. Zhang, M. Pagani, Z. Liu, S. M. Bohaty, R. Deconto, *Philos. Trans. A Math. Phys. Eng. Sci.* **371**, 20130096 (2013).
23. S. Warny *et al.*, *Geology* **37**, 955–958 (2009).
24. A. E. Shevenell, J. P. Kennett, D. W. Lea, *Science* **305**, 1766–1770 (2004).
25. M. J. Kohn *et al.*, *Geology* **32**, 621 (2004).
26. R. E. Dunn *et al.*, *Geol. Soc. Am. Bull.* **125**, 539–555 (2013).
27. L. Hinojosa, *Rev. Geológica Chile* **32**, 95–115 (2005).
28. E. S. Bellosi, in *The Paleontology of Gran Barranca: Evolution and Environmental Change Through the Middle Cenozoic of Patagonia*, R. H. Madden, A. A. Carlini, M. G. Vucetich, R. F. Kay, Eds. (Cambridge Univ Press, Cambridge, UK, 2010), pp. 278–292.
29. S. W. Punyasena, *Palaeogeogr. Palaeoclimatol. Palaeoecol.* **265**, 226–237 (2008).
30. M. H. Ibrahim, H. Z. E. Jaafar, M. H. Harun, M. R. Yusop, *Acta Physiol. Plant.* **32**, 305–313 (2009).
31. R. H. Madden, *Hypsodonty in Mammals: Evolution, Geomorphology and the Role of Earth Surface Processes* (Cambridge Univ. Press, Cambridge, UK, 2014).
32. D. D. Breshears, J. J. Whicker, M. P. Johansen, J. E. Pinder, *Earth Surf. Process. Landf.* **28**, 1189–1209 (2003).
33. L. F. Hinojosa, C. Villagrán, *Palaeogeogr. Palaeoclimatol. Palaeoecol.* **217**, 1–23 (2005).
34. E. S. Bellosi, M. G. Gonzalez, in *The Paleontology of Gran Barranca: Evolution and Environmental Change through the Middle Cenozoic of Patagonia*, R. H. Madden, A. A. Carlini, M. G. Vucetich, R. F. Kay, Eds. (Cambridge Univ. Press, 2010), pp. 293–305.
35. S. Ganguly *et al.*, *Remote Sens. Environ.* **112**, 4318–4332 (2008).
36. E. Gutiérrez, V. Vallejo, *Oecologica Aquat.* **10**, 351–366 (1991).
37. W. Woodgate, *Int. Arch. Photogramm. Remote Sens. Spat. Inf. Sci.* **XXXIX**, 457–462 (2012).
38. G. P. Asner, C. E. Borghi, R. A. Ojeda, *Ecol. Appl.* **13**, 629–648 (2003).
39. M. Barradas, F. Novo (*Folia Geobot. Phytotaxon.* **22**, 415–433 (1987).
40. V. Barraza *et al.*, *IEEE J. Sel. Top. Appl. Earth Obs. Remote Sens.* **7**, 421–430 (2013).

ACKNOWLEDGMENTS

Supplementary data are included in the data file. This research was funded in part by National Science Foundation grants DEB-1110354 to R.E.D. and C.A.E.S. (Doctoral Dissertation Improvement Grant) and EAR-0819910 to C.A.E.S., EAR-0819842 to R.H.M., and EAR-0819837 and EAR-1349749 to M.J.K.; Proyecto de Investigación en Ciencias y Técnicas 1860 of the Fondo Nacional de Ciencia y Tecnología (FONCyT) To A.A.C.; the Geological Society of America; and the University of Washington Department of Biology and Burke Museum of Natural History and Culture. We thank G. Vucetich, M. Ciancio, M. Conner, A. Loeser, Pan American Energy, Organization for Tropical Studies, Área Conservación de Guanacaste, and three reviewers.

SUPPLEMENTARY MATERIALS

www.sciencemag.org/content/347/6219/258/suppl/DC1
Materials and Methods
Figs S1 to S6
Tables S1 to S6
References (*41*–*62*)

8 September 2014; accepted 9 December 2014
10.1126/science.1260947

www.sciencemag.org/content/347/6219/258/suppl/DC1

Supplementary Material for

Linked canopy, climate, and faunal change in the Cenozoic of Patagonia

Regan E. Dunn,* Caroline A. E. Strömberg, Richard H. Madden, Matthew J. Kohn, Alfredo A. Carlini

*Corresponding author. E-mail: dunnr@u.washington.edu

Published 16 January 2015, *Science* **347**, 258 (2015)
DOI: 10.1126/science.1260947

This PDF file includes:

Materials and Methods

Over 200 samples of soil were collected from several locations in protected areas in Costa Rica where land use histories are known including OTS (Organization for Tropical Studies) sites La Selva and Parque Nacional Palo Verde, and sites within the Área de Conservación de Guanacaste including Parque Nacional Santa Rosa, Guanacaste, (Sector Cerro la Hacha), Rincón de La Vieja (Sector Las Pailas), and Puesto San Cristobal. We report on 45 of these samples. Wet tropical forest soils were collected from La Selva, dry tropical forest soils from Santa Rosa, Guanacaste and Palo Verde, flooded forest soils from Palo Verde, and submontane forest samples from Rincon de La Vieja and Puesto San Cristobal (Fig. S1, Table S2).

We chose to conduct our modern calibration experiment in Costa Rica as Patagonian fossil assemblages are non-analogous containing a mixture of Neotropical, subtropical and sub-Antarctic taxa. Of the plant taxa described from two well-known Patagonian floral assemblages (megafloras from the early Eocene Laguna del Hunco sites (*17*) and pollen assemblages from late Oligocene-late Miocene shallow marine deposits (*41*)), around 41% of the genera and 85% of the families grow in Costa Rica today (Table S1). Our study also assumes that cell morphology does not differ with latitudinal differences in photoperiod. To the best of our knowledge, there are no published studies addressing variation in pavement cell morphology with photoperiod. As a result, we make no effort to correct our data for possible latitudinal based variation in cell shape and size. Instead, we assume that relative changes in epidermal phytolith morphology result from canopy-mediated irradiance effects on leaf tissues.

Field Sampling

Sample sites were selected from undisturbed areas. Leaf litter was cleared from the sample sites and the top 1 cm of soil from a 10 x 10 cm area was collected. The resulting collection measured 250 ml in volume. For each collection site, hemispherical photographs were taken using a Nikon CoolPix 4500 camera with attached Nikon Fisheye Converter GC-E8 0.21x lens from a tripod 1 m from the ground. Sampling took place during cloudy days, or in mornings and evenings when the sun was not directly overhead and photographs were taken using the optimum exposure for each site (*42*). Effective Leaf Area Index (L_e) and % canopy openness were measured from the photographs using Gap Light Analyzer (GLA), Version 2.0 imaging software (*43*) L_e is the product of L (the measured LAI) and Ω which is a clumping index resulting from the non-random distribution of element spatial positions such as needles on coniferous trees (*44*). For broad-leaved forests like those sampled in this study, clumping is less of concern and L_e is considered similar to L. The LAI Ring 5 output from GLA was used in this study. It is the effective leaf area index integrated over the zenith angle of 0-75°.

Soil Phytolith Extraction and Analysis

Soil samples were manually homogenized and 1 gram was measured for processing. Extraction of phytoliths was done using modified standard methods of which involve carbonate removal using concentrated HCl, humic acid removal using a 10% KOH solution, organic removal using Schulze's Reagent ($KClO_3$+HNO_3) and removal of oxides with strong acid (equal parts of HCl and HNO_3) (*45*). Sieving removed particles

over 250 μm in diameter, and a finer sieve (56 μm diameter) was used to mechanically break up clays though all size fractions under 250 μm were maintained as one sample. Heavy liquid extraction was performed using a solution of zinc bromide in HCl and water.

For slide preparation, a subset of the sample was mounted on a slide and fixed in Cargille MeltMount™. Slides were scanned in their entirety at 400x magnification and the targeted epidermal phytoliths were located and photographed along slide transects. Selected phytoliths were complete epidermal cells showing the entire outline of the cell. These are easily distinguished from broken phytoliths, which have sharp, angular breakage patterns where lobes are missing. Measurements of cell area and perimeter were made using Adobe Photoshop Extended Version CS5. The Quick Selection Tool was used to outline the cell perimeters, and the relevant measurements of area and perimeter were recorded. In samples where epidermal phytoliths were rare, multiple slides were made to get at least 25 phytoliths per sample.

Distinguishing grass epidermal phytoliths for exclusion

There exists some overlap between wide grass long cells and those considered anticlinal epidermis of non-grass plants. Grass cells were not measured as a part of this study as we have determined in another study that grass cell undulation does not vary with light regime, though cell area and length do. Grass long cells were distinguished from other anticlinals by having Width:Length ratios ≤ 0.67, and by having blunt ends on the short axis (Fig. S2).

Undulation was quantified for each anticlinal phytolith using a unitless measure, the Undulation Index (UI) (*16*). UI is calculated as the circumference of the cell (Ce) divided by the circumference of a circle with the same area (Ae) as the cell (Co).

$$UI = \frac{Ce}{Co} = \frac{Ce}{2\Pi\sqrt{\frac{Ae}{\Pi}}}$$

Quantitative Analyses of Phytoliths

All analyses were done using R version 2.8.1 (*46*). For each site, mean phytolith undulation index (PUI) and phytolith area were calculated. The minimum sample size was determined to be 25 phytoliths/sample through bootstrapping. Mean PUI and phytolith area for each sample were compared to LAI for each site using linear regressions. To develop a statistical model for predicting LAI, a multiple regression including both mean PUI and mean area was performed (mean PUI + Mean Phytolith Area) and 95% confidence intervals were calculated. The formula derived from this

analysis is Eq. 1 in the main text. Statistical output of the model required to calculate confidence intervals are in Table S3.

For the fossil samples, we used Eq. 1 (main text) to calculate rLAI values from mean PUI and mean phytolith area derived from measuring 25-100 individual epidermal phytoliths from each of the fossil extractions. To infer habitat type, we compared the calculated rLAI values to LAI ranges of modern habitats and vegetation types gathered from the literature (Table 1, main text). It should be noted however, that the combination of phytolith composition and rLAI values for many of the fossil samples point to non-analog vegetation types.

Both the raw values for rLAI and bins were plotted against age of the assemblages. Ages for the phytolith samples were determined by the age model used in (*12*) which is based on the geochronology of (*26*)(see Table S4). rLAI bins were grouped according to formation, member or age. These bins were chosen as the formations (Las Flores, Kolhue Kaike fms.) and members of the Sarmiento Fm. (Gran Barranca, Rosado, Lower Puesto Almendra, Vera, Upper Puesto Almendra, and Colhue Huapi) demonstrate distinctive lithologies (Table S4). All of the middle and late Miocene samples (Collon Cura, Rio Negro and Rio Mayo fms.) were binned as they come from several different formations that are close in age.

Study Sites

La Selva Biological Station, Heredia, Costa Rica (10°26'N, 83°59'W), elevation 35-137 m. Holdridge zone: Premontane wet forest (*47*). Annual rainfall exceeds 2000 mm/year with an average of ~4000 mm/year. No month receives less than 100 mm precipitation (*48*). The rainy season is June-July, and Nov-Dec (>400 mm per month). Mean Annual Temperature (MAT) is ~26 °C, and the mean annual daily temperature ranges between 18 and 24°C. The daily range in temperature is 6-12°C. August has the highest temperatures (~27.1°C), and January has the coolest temperatures (24.7°C). Forest canopies at La Selva are a mosaic of different disturbance histories and canopy heights. Trees are the most important functional group (LAI = 3.29) followed by palms (LAI = 1.33) and lianas (LAI = 0.73). Epiphytes, ferns and herbs account for only 11% of the total LAI. LAI values for tall forest sites do not differ from the dry season to the wet season, so LAI is constant throughout the year. Overall landscape LAI that has been measured through destructive sampling is 6.00 +/- 0.32. Of that, trees, palms and lianas account for 89% of the total, and trees and lianas make up 95% of the upper canopy (*49*).

Área Conservacion de Guanacaste-NW Costa Rica

***Parque Nacional Santa Rosa* -** Holdridge Life Zone: semi-deciduous dry tropical forest. Elevation ~300 m. Rainfall is seasonal, between April and November, averaging 1614 mm/year but ranging from 915– 2558 mm/year with a pronounced dry season of 6-months with little to no precipitation (*50*). Mean annual temperature is 27°C with a range of 10°C. The warmest month mean temperature is ~33°C, and the coldest month mean is 21°C. Average temperatures vary between 32–36 °C (*51*). Dominant taxa in the area include *Quercus oleoides*, *Hymenaea courbaril*, and *Manilkara zapota*. These species are not synchronously deciduous (*50*). Soil samples were collected from early, intermediate

and late stage successional plots (*52*). The early successional plots consisted of one canopy layer with an average height of 6 m, containing many deciduous eudicotyledonous taxa, shrubs and grasses. Intermediate successional plots consisted of two canopy layers averaging 10 m in height. Fast growing deciduous species, lianas and a higher proportion of shade tolerant species dominate these plots. Late successional plots (Bosque Humedo) have two layers of canopy averaging 30 m in height. They are dominated by evergreen species with an overlapping canopy. Maximum leaf fall occurs in April at the end of the dry season and maximal LAI values occur in November, though not all species shed their leaves entirely or at the same time. The change in leaf area index between the dry season and wet season is ~40% of the total. Our study was carried out in July when the forest had a continuous cover of leaves (*53*).

Parque Nacional Rincón de La Vieja is an active volcano and several of the Holdridge life zones can be found along its altitudinal gradient including tropical moist forest, premontane wet forest, premontane rain forest, and lower montane rain forest.

Corredor Biológico Puesto San Cristobol - Lower montane and premontane wet forest corredor connecting Pacific and Atlantic forest.

Parque Nacional Guanacaste - Sector Cerro El Hacha – This area is characterized as open savanna with grasses and low shrubs growing on relict volcanic topography. The dominant grass is *Axonopus.*

Curation of Voucher Specimens

All soils, phytolith extracts, and microscope slides are housed at the UW Burke Museum, Seattle, WA in the Paleobotany Collections.

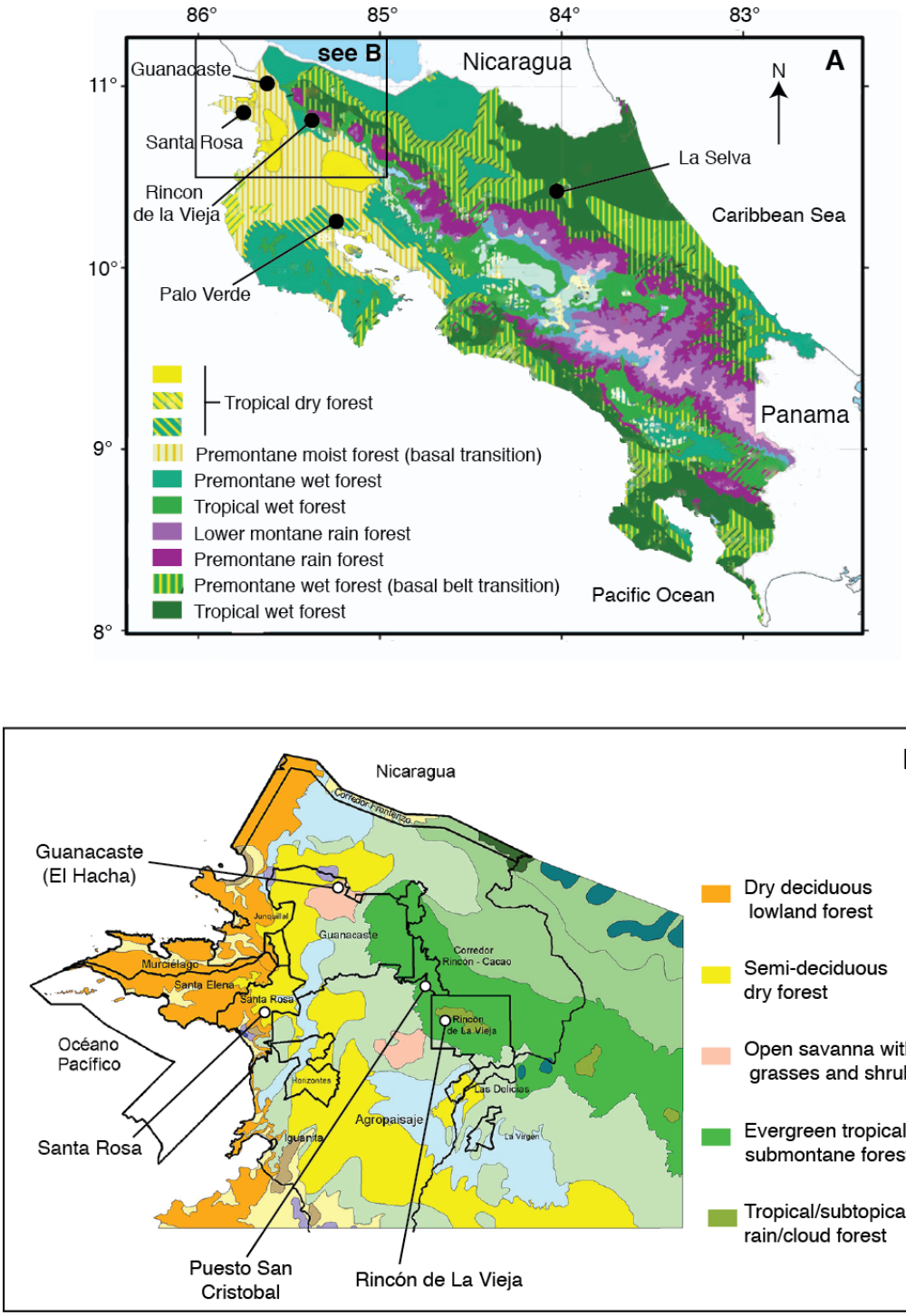

Figure S1. A) Map of sampling areas in Costa Rica along with Holdridge Life Zones. Modified from (*47*, *54*); B) map of vegetation in NW Costa Rica within the Área de Conservacion de Guanacaste. Map made by Waldy Medina, ACG 1999. **http://www.investigadoresacg.org/IMAGES/MAPFILES/maps/physical_biological/vegetacion_acg.jpg**

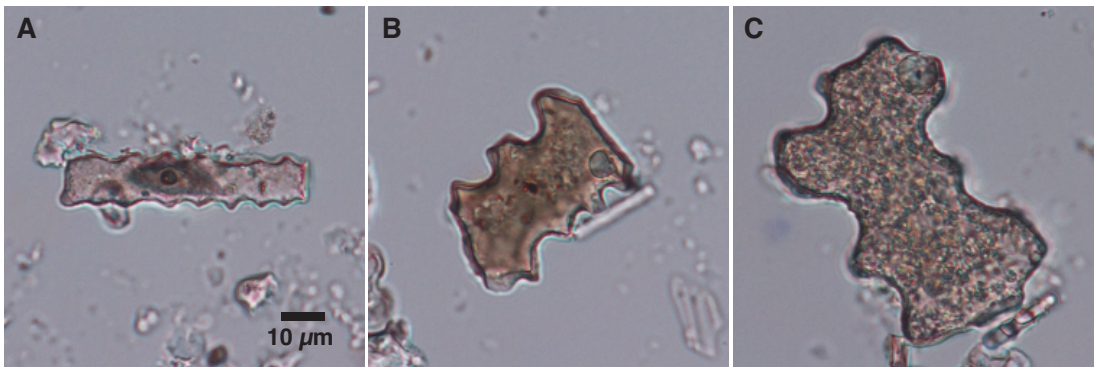

Figure S2. Criteria used to differentiate grass long cells from anticlinal epidermal cells of other taxa. A) Phytolith of grass long cell showing regular, compact undulations, W:L = 0.21, and has blunt ends on the short axis. B) Phytolith of a grass long cell, W:L = 0.64, regular, compact undulations, and has blunt ends on short axis. C) Phytolith of a non-grass anticlinal cell, W:L = 0.67, and has less regular undulations on all sides of cell.

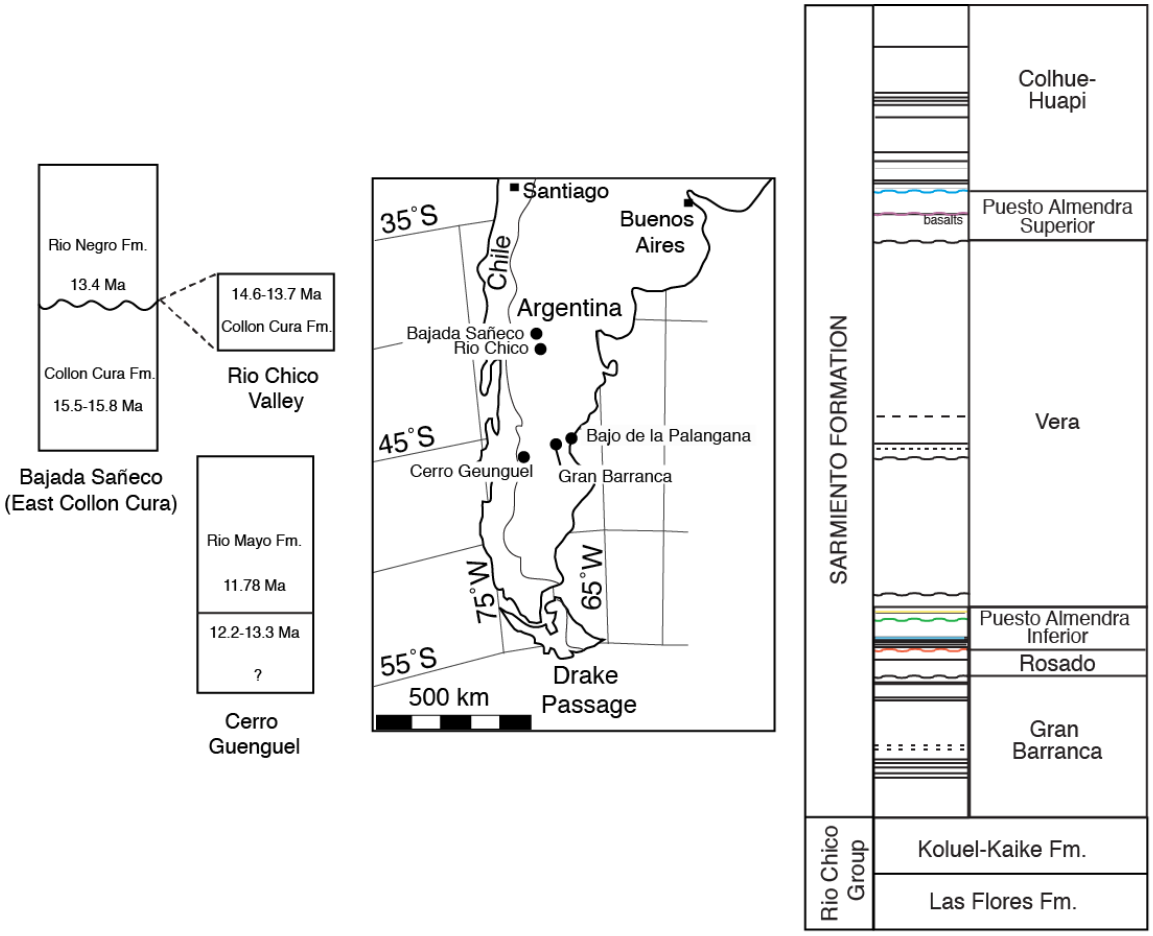

Figure S3. Map showing locations of fossil phytolith samples and generalized stratigraphic sections. Samples of the Sarmiento and Koluel-Kaike formations were collected at Gran Barranca. Las Flores Formation samples were collected at Bajo de la Palangana. Middle Miocene samples were collected at Cerro Guenguel, Bajada Sañeco and in the Rio Chico valley. See Table S4.

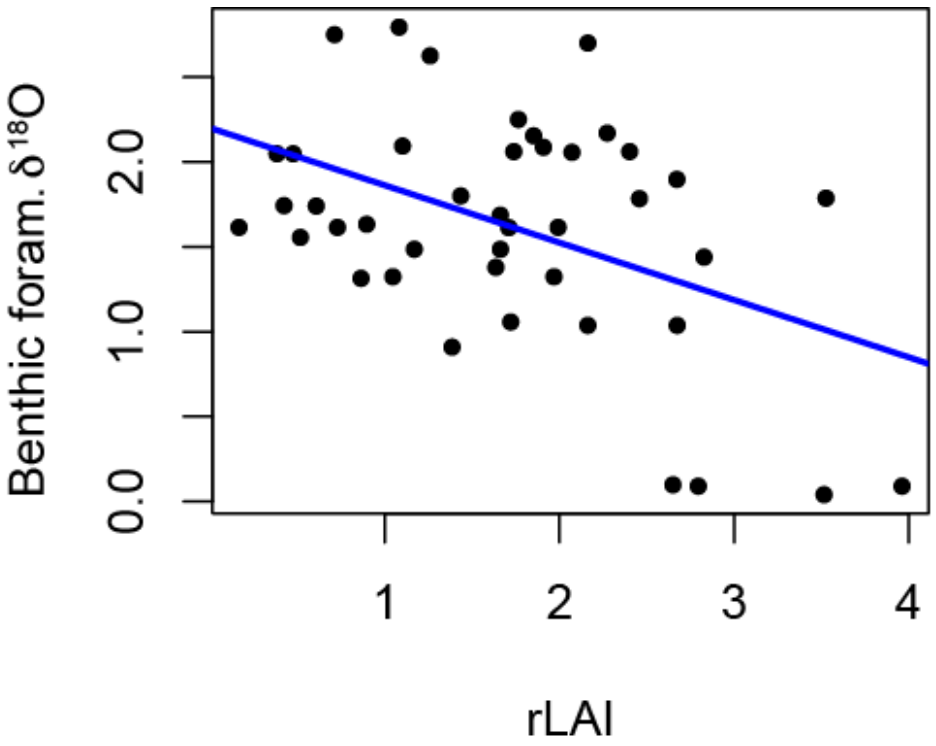

Figure S4. Benthic foraminiferal $\delta^{18}O$ values (*8*) from the Southern Ocean compared to rLAI values (R^2=0.19, p=0.002). $\delta^{18}O$ values represent 10-point averages surrounding estimated age of phytolith sample.

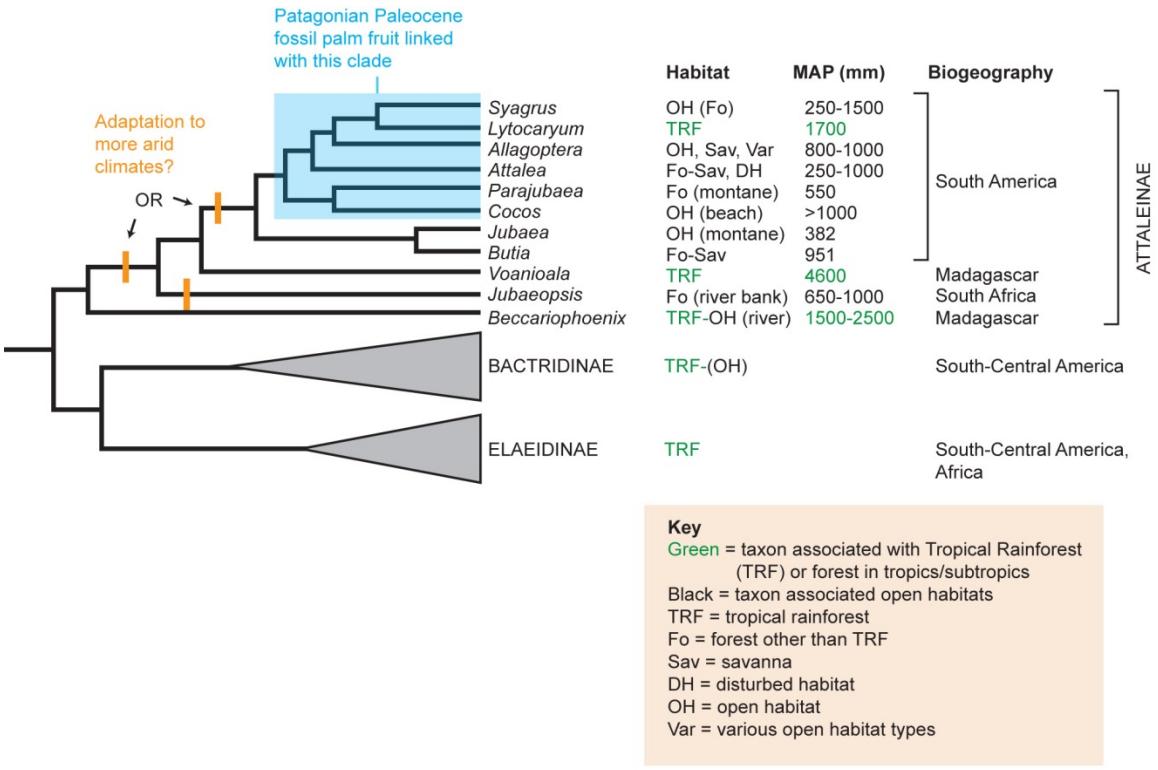

Figure S5. Mapping of habitat preferences of members of the Attaleinae subtribe on the relevant part of the palm (Arecaceae) phylogeny (*55*, *56*) suggests that a tolerance to open habitats or more arid climates occurred early on in this clade. Paleocene fossil palm fruits from Patagonia have links to a clade within this subtribe, and it has been suggested that it was most closely related to *Lytocaryum* (a strict consensus fails to show this relationship; (*57*)). Although *Lytocaryum* itself forms part of tropical rainforest (TRF) vegetation, the phylogenetic placement of the fossils suggests that many of the members of Attaleinae that now occupy non-TRF habitats had diverged by the Paleocene, and that the clade existed in southern South America. We hypothesize that these palms may have thrived in the open, drier vegetation types reconstructed herein. We focus on Attaleinae as the only palm clade that both (a) contains many members that display tolerance to more extreme climates (some drought and cold tolerance) and/or disturbance, and (b) has a distribution in central and southern South America indicating it had its origin there (as opposed to the Caribbean, Central America, and northernmost South America, pointing to a North American origin)(*55*, *56*). Habitat data and MAP from various sources (*58*). Biogeography information from GBIF (http://data.gbif.org/).

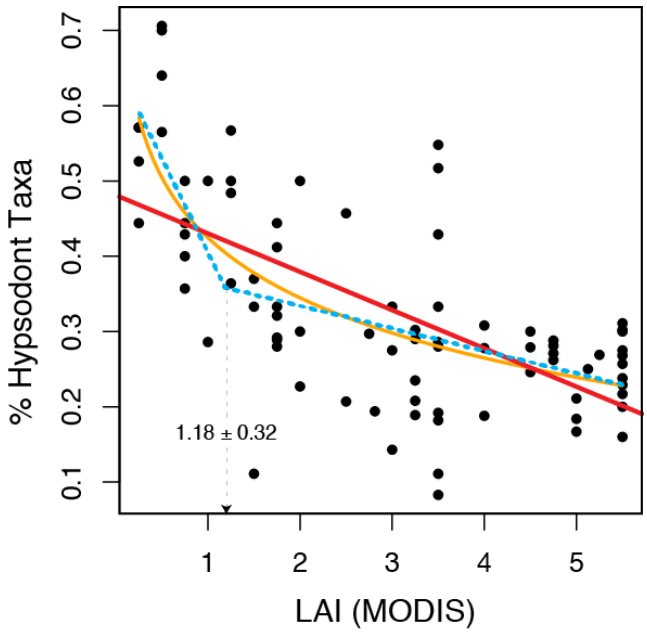

Figure S6. LAI and the prevalence of hypsodonty in living South American mammals. We derived remotely sensed LAI values (MODIS LAI means from 2001-2009) for 80 localities where mammal species inventories have been obtained (Table S7). The percentage of hypsodont mammal species was plotted against LAI values for all species included in the 80 inventories. Several models were fit to the data including linear, log transformed and a segmented regression using the R package "segmented". Hypsodonty is significantly inversely related to LAI in all models ($p<0.0001$). The segmented regression determined a break point at an LAI value of 1.18 ± 0.32. For South American localities, faunal hypsodonty and hypselodonty is the proportion of primary consumers that are high-crowned, and this includes rodents, xenarthrans, and ungulates. In South America, of 474 mammal species that are primary consumers, 191 have either high-crowned or ever-growing cheek teeth. Crown height can be classified for 474 out of 560 (or 85%) of the total number of species. Of these, 191 species (or 40%) were classified as hypsodont (including all xenarthrans). Of the 121 species of Sigmodontinae (Muridae) rodents classified by crown shape, 24 (or 20%) are here considered high-crowned (or here, hypsodont). Sigmodontines were scored as "hypsodont" if they are reported to display greater cheek tooth crown height than found in oryzomyins, the living group most closely related to the presumptive ancestral group (*31*).

Table S1. Tally of shared taxa between fossil sites in Patagonia and extant taxa in Costa Rica.*

	Late Oligocene-late Miocene Pollen[1]	Eocene Laguna del Hunco Megaflora[2]
Genus Level		
Total genera fossil record	46	44
Shared genera extant Costa Rica	18	19
% Shared Genera (Extant Costa Rica & Fossil Record Patagonia)	**39.1**	**43.2**
Family Level		
Total families fossil record	56	35
Shared families extant Costa Rica	49	29
% Shared Families (Extant Costa Rica & Fossil Record Patagonia)	**87.5**	**82.9**

[1]Late Oligocene-Late Miocene sites from (*41*)
[2]Early Eocene Laguna del Hunco sites with some additions. List of taxa and references found here: http://bhort.bh.cornell.edu/histology/taxaLH.html
*A list of taxa will be provided by the corresponding author upon request.

Table S2. Summary data for Costa Rica soil samples.

Site No.	UWBM[1] No.	Veg. type [site]	Sample size	LAI 5[2]	Mean Area (μm^2)	Area SD[3]	Area 95% CI[4]	Mean UI[5]	UI SD	UI 95% CI
RD001	PR08581	wet[LS]	54	2.95	367.84	342.41	91.33	1.44	0.14	0.04
RD007	PR08582	wet[LS]	74	3.88	258.14	281.77	64.20	1.40	0.14	0.03
RD008	PR08583	wet[LS]	65	2.79	781.74	494.18	120.14	1.44	0.18	0.04
RD010	PR08584	wet[LS]	71	2.37	790.12	419.55	97.59	1.39	0.14	0.03
RD011	PR08585	wet[LS]	40	2.73	874.80	586.95	181.89	1.43	0.13	0.04
RD013	PR08586	wet[LS]	42	2.75	924.08	758.48	229.39	1.44	0.15	0.05
RD014	PR08587	wet[LS]	31	2.53	628.09	311.33	109.60	1.51	0.22	0.08
RD016	PR08588	wet[LS]	36	3.09	1143.69	781.93	248.61	1.43	0.15	0.05
RD017	PR08589	wet[LS]	57	3.15	614.40	265.87	69.02	1.48	0.19	0.05
RD021	PR08590	wet[LS]	33	2.39	702.57	523.90	176.10	1.44	0.16	0.05
RD024	PR08591	wet[LS]	36	1.66	940.55	413.80	135.17	1.39	0.13	0.04
RD028	PR08592	wet[LS]	34	3.77	925.32	463.25	155.71	1.42	0.13	0.04
RD029	PR08593	wet[LS]	76	3.29	354.99	502.65	113.01	1.43	0.14	0.03
RD031	PR08594	wet[LS]	66	2.79	846.74	856.00	206.52	1.46	0.15	0.04
RD036	PR08595	wet[LS]	32	4.78	1330.47	1632.34	565.57	1.52	0.26	0.09
RD058	PR08596	wet[LS]	45	3.67	55.98	305.86	89.36	1.47	0.14	0.04
RD066	PR08597	wet[LS]	33	2.44	945.50	421.88	143.94	1.48	0.15	0.05
RD085	PR08598	wet[LS]	49	2.74	575.90	310.09	86.82	1.47	0.12	0.03
RD087	PR08599	wet[LS]	30	3.38	819.50	365.11	130.65	1.50	0.13	0.05
RD089	PR08600	dry[SR]	48	3.96	978.30	391.85	110.85	1.47	0.17	0.05
RD090	PR08601	dry[SR]	42	3.16	931.32	552.21	167.00	1.47	0.17	0.05
RD091	PR08602	dry[SR]	60	4.25	859.84	434.79	129.96	1.48	0.16	0.05
RD093	PR08603	dry[SR]	32	3.65	1026.69	395.75	139.31	1.46	0.16	0.05
RD096	PR08604	dry[SR]	40	2.98	733.63	364.73	113.03	1.50	0.17	0.05
RD099	PR08605	dry[SR]	30	3.35	785.28	292.74	104.76	1.47	0.17	0.06
RD100	PR08606	dry[SR]	47	2.84	1020.60	451.62	129.11	1.50	0.20	0.06
RD102	PR08607	dry[SR]	54	0.16	293.78	155.81	41.56	1.34	0.13	0.04
RD106	PR08608	dry[SR]	52	0.65	288.54	165.47	44.97	1.35	0.15	0.04
RD107	PR08609	dry[SR]	25	1.06	436.71	233.35	95.36	1.34	0.09	0.04
RD127	PR08610	dry[SR]	50	1.29	497.97	717.47	198.87	1.36	0.14	0.04
RD129	PR08611	dry[SR]	57	1.74	549.24	411.05	106.71	1.34	0.11	0.03
RD130	PR08612	dry[SR]	40	1.71	718.50	552.97	171.36	1.37	0.10	0.03
RD131	PR08613	dry[SR]	38	0.73	282.56	240.76	76.55	1.38	0.14	0.05
RD132	PR08614	dry[SR]	25	1.53	642.34	273.77	111.89	1.40	0.15	0.06
RD136	PR08615	dry[SR]	30	1.54	91.92	352.23	126.04	1.36	0.15	0.05
RD138	PR08616	dry[EH]	40	1.04	304.95	231.55	71.76	1.33	0.12	0.04
RD145	PR08617	dry[EH]	25	2.16	767.20	301.24	120.52	1.29	0.08	0.03
RD146	PR08618	dry[EH]	68	0.34	64.88	185.44	44.08	1.33	0.12	0.03
RD149	PR08619	wet[SC]	37	1.98	744.34	405.49	132.46	1.41	0.17	0.05
RD160	PR08620	wet[RV]	31	2.56	14.98	304.38	107.15	1.33	0.10	0.04
RD162	PR08621	wet[RV]	25	2.47	433.84	288.86	113.23	1.41	0.16	0.06
RD174	PR08622	wet[RV]	63	0.33	229.63	222.40	54.92	1.34	0.15	0.04
RD177	PR08623	wet[RV]	64	0.58	274.84	230.45	56.46	1.35	0.14	0.03
RD178	PR08624	wet[RV]	68	1.27	178.11	140.75	33.45	1.28	0.14	0.03
RD180	PR08625	wet[RV]	34	1.19	268.66	170.29	57.24	1.35	0.12	0.04

Notes: [1]UWBM= University of Washington Burke Musuem catalog number, [2]LAI 5 = LAI calculated using 0-75° zenith angle, [3]SD=Standard Deviation, [4]95% Confidence Interval, [5]UI = Undulation Index (see Methods section below). Abbreviations for sites: LS = La Selva; SR = Parque Nacional de Santa Rosa; EH

= El Hacha (Área de Conservación de Guanacaste- ACG); RV = Rincon de la Vieja (ACG); SC = San Cristobal (ACG).

Table S3. Statistical output of rLAI model (Eq. 1).

	Coeff.	Std. Error	t value	Pr(>|t|)
(Intercept)	-1.316e+01	2.857e+00	-4.607	3.77e-05 ***
Area	1.224e-03	4.911e-04	2.493	0.0167 *
UI	1.041e+01	2.162e+00	4.816	1.93e-05 ***

Residual standard error: 0.6952 on 42 degrees of freedom
Multiple R-squared: 0.65, Adjusted R-squared: 0.6333
F-statistic: 39 on 2 and 42 DF, p-value: 2.666e-10

Table S4. Fossil sample data summary.

[1]UWBM no.	[2]Formation/ Member	Age (Ma)	rLAI (m^2/m^2)	95% CI	n	PUI	PA (μm^2)	Binned LAI (m^2/m^2)	Bin Error	Age Reference
PB29347	Rio Mayo	11.78	2.16	0.24	47	1.39	679	2.33	0.51	Madden unpublished
PB39834	Rio Negro	13.40	2.27	1.01	25	1.32	1348			Kohn unpublished
PB29819	Collon Cura	13.70	1.76	0.42	37	1.35	754			Kohn unpublished
PB29817	Collon Cura	13.90	2.67	0.84	42	1.37	1325			Kohn unpublished
PB29812	Collon Cura	14.00	1.43	0.43	66	1.33	646			Kohn unpublished
PB29808	Collon Cura	14.60	3.53	0.44	48	1.47	1155			Kohn unpublished
PB29368	Collon Cura	15.70	2.46	0.61	47	1.37	1099			Madden unpublished
PB29094	Sarmiento CH	18.79	0.57	0.64	25	1.26	523	1.21	0.61	(27)
PB18474	Sarmiento CH	18.814	0.97	0.54	25	1.29	578			(27)
PB18469	Sarmiento CH	20.355	1.91	0.35	85	1.36	735			(27)
PB18467	Sarmiento CH	20.89	1.74	0.36	49	1.35	690			(27)
PB29055	Sarmiento CH	20.907	2.40	0.21	31	1.42	645			(27)
PB29054	Sarmiento CH	21.003	0.38	0.60	33	1.25	399			(27)
PB29052	Sarmiento CH	21.11	0.48	0.56	101	1.26	398			(27)
PB29144	Sarmiento UPA	22.842	1.10	0.44	25	1.31	527	1.57	0.36	(27)
PB18460	Sarmiento UPA	23.130	2.07	0.61	51	1.35	996			(27)
PB29350	Sarmiento	24.1	1.85	0.24	34	1.38	553			Dunn unpublished
PB29133	Sarmiento UPA	27.5	1.59	0.33	62	1.35	605			(27)
PB18458	Sarmiento UPA	30.77	1.26	0.80	42	1.28	911			(27)
PB28354	Sarmiento Vera	33.266	0.71	0.50	59	1.28	429	0.58	0.17	(27)
PB28470	Sarmiento Vera	34.144	0.42	0.61	31	1.25	432			(27)
PB18444	Sarmiento Vera	35.062	0.61	0.55	34	1.27	438			(27)
PB29136	Sarmiento LPA	36.80	1.66	0.66	33	1.32	916	1.42	0.53	(27)
PB18441	Sarmiento LPA	37.408	1.71	0.71	68	1.31	973			(27)
PB18437	Sarmiento LPA	37.798	0.90	0.59	75	1.28	606			(27)
PB18434	Sarmiento Ros.	38.00	0.17	0.83	47	1.21	553	0.43	0.25	(27)
PB28405	Sarmiento Ros.	38.028	0.73	0.57	55	1.27	520			(27)
PB18435	Sarmiento Ros.	38.10	0.52	1.53	41	1.26	483			(27)
PB18433	Sarmiento GB	38.50	0.31	0.53	57	1.27	227			(27)
PB28334	Sarmiento GB	39.057	1.66	0.35	82	1.35	653	1.65	0.36	(27)
PB18430	Sarmiento GB	39.057	1.17	0.53	87	1.30	650			(27)

PB18419	Sarmiento GB	39.80	1.99	0.25	55	1.38	642			(27)
PB18427	Sarmiento GB	39.717	1.05	0.56	50	1.29	635			(27)
PB18428	Sarmiento GB	39.861	0.86	0.66	67	1.27	656			(27)
PB18429	Sarmiento GB	39.449	1.64	0.32	52	1.35	606			(27)
PB18425	Sarmiento GB	39.332	2.83	0.56	28	1.40	1146			(27)
PB18426	Sarmiento GB	39.717	1.97	0.38	64	1.36	776			(27)
PB18421	Sarmiento GB	41.800	1.39	0.38	59	1.33	580			(27)
PB29160	Sarmiento CV	43.000	1.95	0.39	70	1.36	786			Madden unpublished
PB29066	Koluel-Kaike	44.000	2.67	0.22	66	1.44	714	2.19	0.55	(*59*)
PB29149	Koluel-Kaike	44.000	2.16	0.24	60	1.39	679			(*59*)
PB18420	Koluel-Kaike	44.100	1.72	0.99	73	1.43	1186			(*59*)
PB29219	Las Flores	48.900	2.65	0.50	66	1.39	1006	3.23	0.62	(*60*)
PB29217	Las Flores	49.000	3.96	0.92	57	1.45	1655			(*60*)
PB29212	Las Flores	49.100	3.51	0.88	78	1.42	1537			(*60*)
PB29214	Las Flores	49.100	2.79	0.78	65	1.38	1306			(*60*)

Notes: [1]UWBM = University of Washington Burke Museum specimen numbers. [2]Strata of the Sarmiento Formation include the following members in order from oldest to youngest: CV=Canadon Vaca, GB=Gran Barranca, Ros.=Rosado, LPA = Lower Puesto Almendra, Vera, UPA = Upper Puesto Almendra, and CH=Colhue-Haupi.

Table S5. Corrected ages for megafloras in Figure 3C.

Abbrev.	Flora	Age (Ma)	Latitude	Type	Reference
BP	Boca Pupuya	19-10	33°57'	?	(*27*)
LL	Los Litres	21	33°18'	Ar/Ar	(*27*)
G	Goterones	23	33°57'	Sr	(*27*)
NM	Ñirihuau medio	23-19	41°19'	?	(*61*)
LA	Las Aguilas	26-23	33°19'	Ar/Ar	(*27*)
NI	Ñirihuau inferior	28.5-23	41°19'	?	(*61*)
RT	Río Turbio	45-37	51°33'	biostrat.	(*62*)
RP	Río Pichileufú	47.46± 0.05	41°07'	Ar/Ar	(*17*)

Table S6. Summary of faunal data for Patagonian fossil notoungulates used in Figure 3D.

Faunal Level	Age (Ma)	# Taxa	%Hyps	%Elo	%Hyps +Elo	Upper 95% CI*	Lower 95% CI*
Las Flores	49	4	0	0	0	0	0
Vacan CV	43	13	8	0	8	15.4	7.7
Barrancan GB	40	13	8	0	8	15.4	7.7
El Nuevo GB	38.5	11	18	0	18	27.3	18.2
Mustersan GB	38	12	25	0	25	25	25
La Cancha GB	33.6	12	50	0	50	25	25
La Cantera GB	30.8	13	62	15	77	23.1	23.1
Deseadan CB+LF	24.1	16	63	25	88	12.5	18.6
Colhuehuapian GB	20.9	4	75	25	100	0	0
Pinturan (GB)	19.2	3	0	100	100	0	0
Pinturan SALMA	17	3	0	100	100	0	0
Santa Cruz	16	6	33	50	83	16.7	33.3
Cerro Boleadoras	16	4	25	50	75	25	50
Collon-Cura	15.7	4	0	100	100	0	0
Rio Chico	14.6	4	0	100	100	0	0
Mayoan	11.8	3	0	100	100	0	0

Notes: Abbreviations- CV = Cañadon Vaca; CB= Cabeza Blanca; GB = Gran Barranca; LF = La Flecha. *95% confidence intervals based on bootstrapping analysis using the package “bootstrap” in R statistical software R version 2.8.1 (*49*).

Table S7. Data from modern South American sites relating mean LAI values derived from MODIS (2000-2009) and percent of mammalian species in faunal inventories with hypsodont tooth morphologies.

Site	Latitude	Longitude	Country	LAI	% Hypso.
TIERRA DEL FUEGO	54.660	68.500	Argentina	1	28.6
GLACIARES (LOS)	50.000	73.170	Argentina	0.75	50
PERITO MORENO	47.950	72.250	Argentina	1.25	50
BOSQUE PETRIFICADO	47.680	68.170	Argentina	0.25	52.6
ALERCES (LOS)	42.850	71.850	Argentina	3.5	33.3
PUELO (LAGO)	42.160	71.670	Argentina	3	33.3
NAHUEL HUAPI	41.220	71.500	Argentina	3.5	54.8
ARRAYANES (LOS)	40.830	71.630	Argentina	3.5	42.9
LANIN	39.630	71.500	Argentina	3.5	51.7
LAGUNA BLANCA (P.N.)	39.030	70.350	Argentina	0.75	42.9
LIHUE CALEL	37.960	65.620	Argentina	0.75	40
OTAMENDI	34.230	58.850	Argentina	1.75	28
MENDOZA (Monte)	33.000	68.520	Argentina	0.25	44.4
QUIJADAS (SIERRA DE LAS)	32.480	67.030	Argentina	0.5	56.5
PALMAR (EL)	31.900	58.250	Argentina	1.5	37
LEONCITO (EL)	31.760	69.330	Argentina	0.25	57.1
DIAMANTE	31.750	60.720	Argentina	1	50
MBURUCUYA	28.020	58.020	Argentina	1.75	29.2
COLONIA BENITEZ	27.420	58.930	Argentina	2	50
MISIONES	27.000	54.300	Argentina	4	18.8
CHACO	26.500	59.500	Argentina	2	30
SAN ANTONIO	26.080	53.760	Argentina	3.25	29
SALTAMonte	26.000	66.000	Argentina	0.75	35.7
IGUAZU	25.630	54.330	Argentina	3.25	23.5
RIO PILCOMAYO	25.070	58.160	Argentina	1.75	28.9
REY (EL)	24.670	64.670	Argentina	2.5	20.7
FORMOSA	24.320	61.750	Argentina	1.25	48.4
CALILEGUA	23.700	64.780	Argentina	3.5	28
CALILEGUA 550m Caimancito	23.700	64.670	Argentina	3.5	11.1
CALILEGUA 600m Aguas Negras	23.900	64.930	Argentina	3.5	18.2
CALILEGUA 1150m Mesada de las Colmenas	23.800	65.030	Argentina	3.5	8.3
CALILEGUA 1700m Abra de Cañas	23.780	65.100	Argentina	3.5	19.2
CALILEGUA 2500m Duraznillar	23.570	64.920	Argentina	3.5	28.6
CALILEGUA 2800m Cerro Hermoso Praderas	23.580	64.870	Argentina	0.75	44.4
SALTA- Puna	24.580	67.420	Argentina	0.5	70.6
SALTA- Upper Montane	25.600	65.630	Argentina	1.5	11.1
SALTA- Low Montane	24.680	64.250	Argentina	3.25	20.8
SALTA- Transitional	22.270	63.730	Argentina	3.25	30.2
SALTA-Chaco	24.180	62.880	Argentina	2.5	45.7
BARITU	22.580	64.700	Argentina	3.25	18.9
EDUARDO ABAROA	22.470	67.480	Bolivia	0.25	57.1
Perforacion	19.920	62.570	Bolivia	1.75	44.4
Curuyuqui	18.750	62.220	Bolivia	1.75	41.2
HUAJARA	17.930	67.100	Bolivia	0.5	64
Acurizal	17.750	57.620	Brazil	3	27.5
BOLIVIA Puna	17.000	68.000	Bolivia	1.25	56.7
ISIBORO-SECURE	16.150	66.070	Bolivia	4.5	24.6
PERU Puna	16.000	70.000	Peru	0.5	70

BOLIVIA Ceja	16.000	68.000	Bolivia	2.81	19.4
Federal District	15.950	47.900	Brazil	1.5	33.3
BOLIVIA Yungas	15.000	67.500	Bolivia	5	16.7
PILON LAJAS	14.910	67.280	Bolivia	5	18.4
Alto Madidi	13.670	68.750	Bolivia	5	21.1
Tambopata	13.330	69.630	Peru	4.75	27.1
Explorers Inn	12.830	69.280	Peru	5.5	30.2
Rio Heath	12.830	68.820	Bolivia	5.5	31.1
Cuzco Amazonico	12.550	69.050	Peru	5.5	25.7
BOLIVIA-Tropical	12.000	67.500	Bolivia	5.5	20
PERU-Cocha Cashu	11.920	71.300	Peru	5.13	25
Manuripi-Heath	11.660	67.500	Bolivia	5.5	21.7
Balta	10.130	71.220	Peru	5.5	26.8
Caatingas	7.520	39.720	Brazil	1.25	36.4
Rio Cenepa	4.780	78.280	Peru	4.75	28.8
Xingu	3.650	52.370	Brazil	4.5	30
ECUADOR-Temperate	3.000	79.000	Ecuador	3	14.3
Manaus	2.500	60.000	Brazil	5.5	30
ECUADOR-Subtropical	1.500	78.000	Ecuador	5.5	16
ECUADOR-Tropical	1.500	76.500	Ecuador	5.5	27.5
ECUADOR-Mera	1.450	78.120	Ecuador	5.5	22.9
Belem	1.450	48.480	Brazil	4.75	26.2
ECUADOR-Andean	1.000	78.600	Ecuador	2	22.7
Esmeralda	3.080	65.580	Venezuela	5.5	23.8
Nouragues	4.080	52.670	Guyane	4.75	28.1
Raleigh-Voltzberg	4.750	56.000	Suriname	5.25	26.9
Puerto Ayacucho	5.250	67.670	Venezuela	4.5	27.9
Puerto Páez	6.380	67.480	Venezuela	1.75	33.3
Kartabo	6.380	58.680	Guyana	4	27.8
Nulita	7.320	71.950	Venezuela	4	30.8
Masaguaral	8.570	67.580	Venezuela	1.75	32.1
Guatopo	10.000	66.000	Venezuela	2.75	29.7

References and Notes

1. G. P. Asner, J. M. O. Scurlock, J. A. Hicke, Global synthesis of leaf area index observations: Implications for ecological and remote sensing studies. *Glob. Ecol. Biogeogr.* **12**, 191–205 (2003). doi:10.1046/j.1466-822X.2003.00026.x

2. R. F. Kay, R. H. Madden, C. Van Schaik, D. Higdon, Primate species richness is determined by plant productivity: Implications for conservation. *Proc. Natl. Acad. Sci. U.S.A.* **94**, 13023–13027 (1997). Medline doi:10.1073/pnas.94.24.13023

3. R. Betts, P. Cox, S. Lee, F. Woodward, Contrasting physiological and structural vegetation feedbacks in climate change simulations. *Nature* **387**, 796–799 (1997). doi:10.1038/42924

4. O. Dermody, J. F. Weltzin, E. C. Engel, P. Allen, R. J. Norby, How do elevated [CO_2], warming, and reduced precipitation interact to affect soil moisture and LAI in an old field ecosystem? *Plant Soil* **301**, 255–266 (2007). doi:10.1007/s11104-007-9443-x

5. A. Iio, K. Hikosaka, N. P. R. Anten, Y. Nakagawa, A. Ito, Global dependence of field-observed leaf area index in woody species on climate: A systematic review. *Glob. Ecol. Biogeogr.* **23**, 274–285 (2013). doi:10.1111/geb.12133

6. A. C. Staver, S. Archibald, S. A. Levin, The global extent and determinants of savanna and forest as alternative biome states. *Science* **334**, 230–232 (2011). Medline doi:10.1126/science.1210465

7. Materials and methods are available as supplementary materials on *Science* Online.

8. J. Zachos, M. Pagani, L. Sloan, E. Thomas, K. Billups, Trends, rhythms, and aberrations in global climate 65 Ma to present. *Science* **292**, 686–693 (2001). Medline doi:10.1126/science.1059412

9. R. Livermore, C.-D. Hillenbrand, M. Meredith, G. Eagles, Drake Passage and Cenozoic climate: An open and shut case? *Geochem. Geophys. Geosyst.* **8**, Q01005 (2007). doi:10.1029/2005GC001224

10. M. Pagani, J. C. Zachos, K. H. Freeman, B. Tipple, S. Bohaty, Marked decline in atmospheric carbon dioxide concentrations during the Paleogene. *Science* **309**, 600–603 (2005). Medline doi:10.1126/science.1110063

11. B. F. Jacobs, J. D. Kingston, L. L. Jacobs, The origin of grass-dominated ecosystems. *Ann. Mo. Bot. Gard.* **86**, 590–643 (1999). doi:10.2307/2666186

12. C. A. E. Strömberg, R. E. Dunn, R. H. Madden, M. J. Kohn, A. A. Carlini, Decoupling the spread of grasslands from the evolution of grazer-type herbivores in South America. *Nat. Commun.* **4**, 1478 (2013). Medline doi:10.1038/ncomms2508

13. C. A. E. Strömberg, Using phytolith assemblages to reconstruct the origin and spread of grass-dominated habitats in the great plains of North America during the late Eocene to early Miocene. *Palaeogeogr. Palaeoclimatol. Palaeoecol.* **207**, 239–275 (2004). doi:10.1016/j.palaeo.2003.09.028

14. L. Bremond, A. Alexandre, C. Hély, J. Guiot, A phytolith index as a proxy of tree cover density in tropical areas: Calibration with leaf area index along a forest-savanna transect

in southeastern Cameroon. *Global Planet. Change* **45**, 277–293 (2005). doi:10.1016/j.gloplacha.2004.09.002

15. R. W. Watson, The effect of cuticular hardening on the form of epidermal cells. *New Phytol.* **41**, 223–229 (1942). doi:10.1111/j.1469-8137.1942.tb07075.x

16. W. M. Kürschner, The anatomical diversity of recent and fossil leaves of the durmast oak (*Quercus petraea* Lieblein/*Q. pseudocastanea* Goeppert)—Implications for their use as biosensors of palaeoatmospheric CO_2 levels. *Rev. Palaeobot. Palynol.* **96**, 1–30 (1997). doi:10.1016/S0034-6667(96)00051-6

17. P. Wilf, K. R. Johnson, N. R. Cúneo, M. E. Smith, B. S. Singer, M. A. Gandolfo, Eocene plant diversity at Laguna del Hunco and Río Pichileufú, Patagonia, Argentina. *Am. Nat.* **165**, 634–650 (2005). Medline doi:10.1086/430055

18. V. Barreda, L. Palazzesi, Patagonian vegetation turnovers during the Paleogene-Early Neogene: Origin of arid-adapted floras. *Bot. Rev.* **73**, 31–50 (2007). doi:10.1663/0006-8101(2007)73[31:PVTDTP]2.0.CO;2

19. E. J. Romero, Paleogene phytogeography and climatology of South America. *Ann. Mo. Bot. Gard.* **73**, 449–461 (1986). doi:10.2307/2399123

20. L. Palazzesi, V. Barreda, Fossil pollen records reveal a late rise of open-habitat ecosystems in Patagonia. *Nat. Commun.* **3**, 1294 (2012). Medline doi:10.1038/ncomms2299

21. S. M. Bohaty, J. C. Zachos, Significant Southern Ocean warming event in the late middle Eocene. *Geology* **31**, 1017–1020 (2003). doi:10.1130/G19800.1

22. Y. G. Zhang, M. Pagani, Z. Liu, S. M. Bohaty, R. Deconto, A 40-million-year history of atmospheric CO_2. *Philos. Trans. A Math. Phys. Eng. Sci.* **371**, 20130096 (2013). Medline doi:10.1098/rsta.2013.0096

23. S. Warny, R. A. Askin, M. J. Hannah, B. A. R. Mohr, J. I. Raine, D. M. Harwood, F. Florindo, Palynomorphs from a sediment core reveal a sudden remarkably warm Antarctica during the middle Miocene. *Geology* **37**, 955–958 (2009). doi:10.1130/G30139A.1

24. A. E. Shevenell, J. P. Kennett, D. W. Lea, Middle Miocene Southern Ocean cooling and Antarctic cryosphere expansion. *Science* **305**, 1766–1770 (2004). Medline doi:10.1126/science.1100061

25. M. J. Kohn, J. A. Josef, R. Madden, R. Kay, G. Vucetich, A. A. Carlini, Climate stability across the Eocene-Oligocene transition, southern Argentina. *Geology* **32**, 621 (2004). doi:10.1130/G20442.1

26. R. E. Dunn, R. H. Madden, M. J. Kohn, M. D. Schmitz, C. A. E. Stromberg, A. A. Carlini, G. H. Re, J. Crowley, A new chronology for middle Eocene-early Miocene South American Land Mammal Ages. *Geol. Soc. Am. Bull.* **125**, 539–555 (2013). doi:10.1130/B30660.1

27. L. Hinojosa, Climatic and vegetational changes inferred from southern South America Cenozoic paleoflora. *Rev. Geológica Chile* **32**, 95–115 (2005).

28. E. S. Bellosi, in *The Paleontology of Gran Barranca: Evolution and Environmental Change Through the Middle Cenozoic of Patagonia*, R. H. Madden, A. A. Carlini, M. G. Vucetich, R. F. Kay, Eds. (Cambridge Univ Press, Cambridge, UK, 2010), pp. 278–292.

29. S. W. Punyasena, Estimating Neotropical palaeotemperature and palaeoprecipitation using plant family climatic optima. *Palaeogeogr. Palaeoclimatol. Palaeoecol.* **265**, 226–237 (2008). doi:10.1016/j.palaeo.2008.04.025

30. M. H. Ibrahim, H. Z. E. Jaafar, M. H. Harun, M. R. Yusop, Changes in growth and photosynthetic patterns of oil palm (*Elaeis guineensis* Jacq.) seedlings exposed to short-term CO_2 enrichment in a closed top chamber. *Acta Physiol. Plant.* **32**, 305–313 (2009). doi:10.1007/s11738-009-0408-y

31. R. H. Madden, *Hypsodonty in Mammals: Evolution, Geomorphology and the Role of Earth Surface Processes* (Cambridge Univ. Press, Cambridge, UK, 2014).

32. D. D. Breshears, J. J. Whicker, M. P. Johansen, J. E. Pinder, Wind and water erosion and transport in semi-arid shrubland, grassland and forest ecosystems: Quantifying dominance of horizontal wind-driven transport. *Earth Surf. Process. Landf.* **28**, 1189–1209 (2003). doi:10.1002/esp.1034

33. L. F. Hinojosa, C. Villagrán, Did South American Mixed Paleofloras evolve under thermal equability or in the absence of an effective Andean barrier during the Cenozoic? *Palaeogeogr. Palaeoclimatol. Palaeoecol.* **217**, 1–23 (2005). doi:10.1016/j.palaeo.2004.11.013

34. E. S. Bellosi, M. G. Gonzalez, in *The Paleontology of Gran Barranca: Evolution and Environmental Change through the Middle Cenozoic of Patagonia*, R. H. Madden, A. A. Carlini, M. G. Vucetich, R. F. Kay, Eds. (Cambridge Univ. Press, 2010), pp. 293–305.

35. S. Ganguly, A. Samanta, M. Schull, N. Shabanov, C. Milesi, R. Nemani, Y. Knyazikhin, R. Myneni, Generating vegetation leaf area index Earth system data record from multiple sensors. Part 2: Implementation, analysis and validation. *Remote Sens. Environ.* **112**, 4318–4332 (2008). doi:10.1016/j.rse.2008.07.013

36. E. Gutiérrez, V. Vallejo, R. J, J. Fons, The subantarctic Nothofagus forests of Tierra del Fuego: Distribution, structure and production. *Oecologica Aquat.* **10**, 351–366 (1991).

37. W. Woodgate, An intercomparison of passive terrestrial remote sensing technologies to derive LAI and canopy cover metrics. *Int. Arch. Photogramm. Remote Sens. Spat. Inf. Sci.* **XXXIX**, 457–462 (2012). doi:10.5194/isprsarchives-XXXIX-B8-457-2012

38. G. P. Asner, C. E. Borghi, R. A. Ojeda, Desertification in Central Argentina: Changes in ecosystem carbon and nitrogen from imaging spectroscopy. *Ecol. Appl.* **13**, 629–648 (2003). doi:10.1890/1051-0761(2003)013[0629:DICACI]2.0.CO;2

39. M. Barradas, F. Novo, The vertical structure of Mediterranean scrub in Doñana National Park, (SW Spain). *Folia Geobot. Phytotaxon.* **22**, 415–433 (1987).

40. V. Barraza, F. Grings, P. Ferrazzoli, M. Salvia, M. Maas, R. Rahmoune, C. Vittucci, H. Karszenbaum, Monitoring vegetation moisture using passive microwave and optical indices in the Dry Chaco. *IEEE J. Sel. Top. Appl. Earth Obs. Remote Sens.* **7**, 421–430 (2013). doi:10.1109/JSTARS.2013.2268011

41. V. D. Barreda, L. Palazzesi, in *Paleobotany and Biogeography: A Festschrift for Alan Graham in His 80th Year*, P. H. Stevens, W. D. Montiel, O. M. Raven, Eds. (Missouri Botanical Garden Press, St. Louis, 2014), pp. 1–25.

42. Y. Zhang, J. M. Chen, J. R. Miller, Determining digital hemispherical photograph exposure for leaf area index estimation. *Agric. For. Meteorol.* **133**, 166–181 (2005). doi:10.1016/j.agrformet.2005.09.009

43. G. Frazer, C. Canham, K. Lertzman, Gap Light Analyzer (GLA), version 2.0: Imaging software to extract canopy structure and gap light transmission indices from true-colour fisheye photographs, users manual and program documentation. *Simon Fraser Univ.* (1999); available at http://rem.sfu.ca/forestry/downloads/Files/GLAV2UsersManual.pdf.

44. J. M. Chen, T. Black, R. S. Adams, Evaluation of hemispherical photography for determining plant area index and geometry of a forest stand. *Agric. For. Meteorol.* **56**, 129–143 (1991). doi:10.1016/0168-1923(91)90108-3

45. Z. Zhao, D. M. Pearsall, Experiments for improving phytolith extraction from soils. *J. Archaeol. Sci.* **25**, 587–598 (1998). doi:10.1006/jasc.1997.0262

46. The R Core Team, *et al.*, R: A language and environment for statistical computing (R Foundation for Statistical Computing, Vienna, Austria, 2005).

47. L. Holdridge, W. Grenke, *Forest Environments in Tropical Life Zones: A Pilot Study* (Pergamon, Oxford, UK, 1971).

48. R. L. Sanford Jr., P. Paaby, J. C. Luvall, E. Phillips, Climate, geomorphology, and aquatic systems. *La Selva Ecol. Nat. Hist. a Neotrop. rain For. Univ. Chicago Press. Chicago, Illinois, USA*, 19–33 (1994).

49. D. B. Clark, P. C. Olivas, S. F. Oberbauer, D. A. Clark, M. G. Ryan, First direct landscape-scale measurement of tropical rain forest Leaf Area Index, a key driver of global primary productivity. *Ecol. Lett.* **11**, 163–172 (2008). Medline

50. R. Burnham, Stand characteristics and leaf litter composition of a dry forest hectare in Santa Rosa National Park, Costa Rica. *Biotropica* **29**, 384–395 (2006). doi:10.1111/j.1744-7429.1997.tb00034.x

51. D. Janzen, in *Caterpillars: Ecological and Evolutionary Constraints on Foraging*, N. E. Stamp, T. M. Casey, Eds. (Chapman and Hall, New York, USA, 1993), pp. 448–477.

52. M. Kalacska, G. A. Sanchez-Azofeifa, J. C. Calvo-Alvarado, M. Quesada, B. Rivard, D. H. Janzen, Species composition, similarity and diversity in three successional stages of a seasonally dry tropical forest. *For. Ecol. Manage.* **200**, 227–247 (2004). doi:10.1016/j.foreco.2004.07.001

53. M. Kalácska, J. C. Calvo-Alvarado, G. A. Sánchez-Azofeifa, Calibration and assessment of seasonal changes in leaf area index of a tropical dry forest in different stages of succession. *Tree Physiol.* **25**, 733–744 (2005). Medline doi:10.1093/treephys/25.6.733

54. B. Kohlmann *et al.*, Biodiversity conservation in Costa Rica: A correspondence analysis between identified biodiversity hotspots (Araceae, Arecaceae, Bromeliaceae, and Scarabaeinae) and conservation priority life zones. *Rev. Mex. Biodivers.* **81**, 511–559 (2010).

55. W. J. Baker, T. L. P. Couvreur, Global biogeography and diversification of palms sheds light on the evolution of tropical lineages. I. Historical biogeography. *J. Biogeogr.* **40**, 274–285 (2013). doi:10.1111/j.1365-2699.2012.02795.x

56. W. Baker, T. Couvreur, Global biogeography and diversification of palms sheds light on the evolution of tropical lineages. II. Diversification history and origin of regional assemblages. *J. Biogeogr.* **40**, 286–298 (2013). doi:10.1111/j.1365-2699.2012.02794.x

57. M. K. Futey, M. A. Gandolfo, M. C. Zamaloa, R. Cúneo, G. Cladera, Arecaceae fossil fruits from the Paleocene of Patagonia, Argentina. *Bot. Rev.* **78**, 205–234 (2012). doi:10.1007/s12229-012-9100-9

58. T. L. P. Couvreur, F. Forest, W. J. Baker, Origin and global diversification patterns of tropical rain forests: Inferences from a complete genus-level phylogeny of palms. *BMC Biol.* **9**, 44 (2011). Medline doi:10.1186/1741-7007-9-44

59. W. C. Clyde, P. Wilf, A. Iglesias, R. L. Slingerland, T. Barnum, P. K. Bijl, T. J. Bralower, H. Brinkhuis, E. E. Comer, B. T. Huber, M. Ibanez-Mejia, B. R. Jicha, J. M. Krause, J. D. Schueth, B. S. Singer, M. S. Raigemborn, M. D. Schmitz, A. Sluijs, M. C. Zamaloa, New age constraints for the Salamanca Formation and lower Rio Chico Group in the western San Jorge Basin, Patagonia, Argentina: Implications for Cretaceous-Paleogene extinction recovery and land mammal age correlations. *Geol. Soc. Am. Bull.* **126**, 289–306 (2014). doi:10.1130/B30915.1

60. M. O. Woodburne, F. J. Goin, M. S. Raigemborn, M. Heizler, J. N. Gelfo, E. V. Oliveira, Revised timing of the South American early Paleogene land mammal ages. *J. S. Am. Earth Sci.* **54**, 109–119 (2014). doi:10.1016/j.jsames.2014.05.003

61. R. Giacosa, J. Afonso, N. Herediac, J. Paredes, Tertiary tectonics of the sub-Andean region of the North Patagonian Andes, southern central Andes of Argentina (41–42°30′S). *J. S. Am. Earth Sci.* **20**, 157–170 (2005). doi:10.1016/j.jsames.2005.05.013

62. N. Malumián, A. Caramés, Upper Campanian-Paleogene from the Río Turbio coal measures in southern Argentina: Micropaleontology and the Paleocene/Eocene boundary. *J. S. Am. Earth Sci.* **10**, 189–201 (1997). doi:10.1016/S0895-9811(97)00015-1